Multiscale Model. Simul.
Vol. 10, No. 3, pp. 936–953

DYNAMICS OF A FAULT STEADILY PROPAGATING WITHIN A STRUCTURAL INTERFACE*

G. S. MISHURIS†, A. B. MOVCHAN‡, AND D. BIGONI§

Abstract. Analysis of propagation of a fault driven by a steadily moving shearing force through a structural interface reveals a channeling effect for the energy release. This effect implies that a steady-state solution for propagation exists, but, differently from the case of fault propagation in an infinite lattice, it turns out to always be unstable at low velocity and for fixed load, while stability can be achieved at high propagation velocity only if the amplitude load becomes a specially "designed" decreasing function of the velocity. With a proper choice of this load application law, the propagation can even be stopped. The disclosed behavior also contrasts with the solution for the propagation of a fracture in a homogeneous linearly elastic medium, where for fixed load the crack initially moves and later comes to a stop.

Key words. steady-state crack propagation, discrete lattice, Wiener–Hopf equation, Bloch–Floquet analysis

AMS subject classifications. 37K69, 37L60, 45E10, 74H05, 74H15, 74J05

DOI. 10.1137/110845732

1. Introduction.

Structural interfaces, namely, discrete structures joining continuous media, are a model for the accurate description of several mechanical systems at different scales (Bigoni and Movchan (2002); Movchan, Bullough, and Willis (2003)). These interfaces have been shown to introduce unchallenged mechanical properties for quasi-static (Bertoldi, Bigoni, and Drugan (2007a,b)) and dynamic (Brun, Movchan, and Movchan (2010); Gei (2008)) loading. The analysis of failure within a structural interface is a problem of great interest, since discrete structures are known to yield relief of stress concentration (Bertoldi, Bigoni, and Drugan (2007c)), but their behavior at failure is still unexplored.

Modeling of fracture in an infinite lattice has been initiated by Slepyan (2002, 2005) and extended in different directions by Movchan and Slepyan (2007) and Mishuris, Movchan, and Slepyan (2008, 2009). Lattice Green's functions have been analyzed by Martinsson and Rodin (2002) and Martin (2006) and applications to subcritical crack growth given by Zhao, Makarov, and Rodin (2011). Our interest in the present article is to develop a model for a fault propagating through a structural interface, which consists of an infinite periodic chain of elastic elements. These elements fail when a certain maximum displacement is attained and the fault is propagated through a steadily moving force. Since our structural interface is an "isolated" structure, not connected to infinite media, a channeling effect is observed, so that en-

*Received by the editors August 25, 2011; accepted for publication (in revised form) April 30, 2012; published electronically August 21, 2012.
http://www.siam.org/journals/mms/10-3/84573.html
†Institute of Mathematics and Physics, Aberystwyth University, Aberystwyth SY23 3BZ, UK (ggm@aber.ac.uk, http://www.aber.ac.uk/en/imaps/staff-list/ggm/). This author's work was supported by FP7 research project PIAP-GA-284555-PARM-2.
‡Department of Mathematical Sciences, University of Liverpool, Liverpool L69 3BX, UK (abm@liv.ac.uk, http://www.maths.liv.ac.uk/∼abm/). This author's work was supported by FP7 research project PIAP-GA-284555-PARM-2.
§Department of Mechanical and Structural Engineering, University of Trento, I-38050 Trento, Italy (bigoni@ing.unitn.it, http://www.ing.unitn.it/∼bigoni/). This author's work was supported by Italian Cofin 2009 "2009XWLFKW-002."

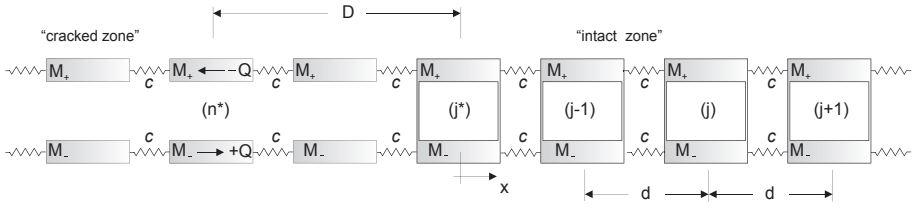

FIG. 1. *Shear-type structural interface, with concentrated forces applied at n^* and faulted up to the position j^*, so that the distance between n^* and j^* is denoted by D.*

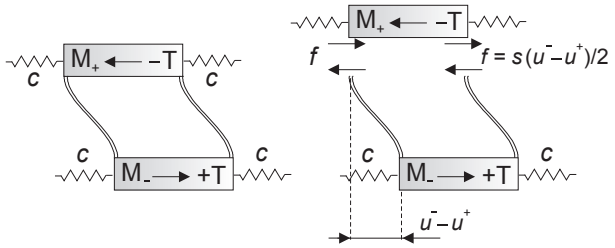

FIG. 2. *Shear-type response of the single cell forming the structural interface shown in Figure* 1.

ergy cannot "escape" and, as a consequence, fault propagation is always found to be unstable, a behavior contrasting with the situation of crack propagation in an infinite lattice and also in an elastic material, two cases in which the propagation is always stable (steady in the former situation, with decreasing velocity in the latter). A way to enforce stability of propagation at high propagation (subsonic) speed is also found, and it consists of a decrease of the amplitude of the applied load, following a certain law.

The present article is organized as follows. After the structural interface model is formulated (section 2), a continuous model for the structural interface is developed and solved for quasi-static and dynamical loading in section 3, where also the discrete model of the interface is solved in both the static and dynamic regimes. The latter situation is addressed with a Wiener–Hopf technique. Numerical results close the article (section 4).

2. Problem formulation. We consider the dynamic response of a unidimensional, infinite, and periodic structural interface formed by a chain of "cells." These are made up of two rows of masses connected horizontally by longitudinal springs of stiffness c and vertically by transversal springs of stiffness s (Figures 1 and 2). The geometry of the chain is such that if $x = 0$ denotes the center of the jth mass, the centers of all masses are located at $x + n\,d$, with n taking values within the set of all integers. Masses on the upper (lower) row are denoted by M_+ (M_-), and the single cell forming the chain has the shear-type behavior sketched in Figure 2, so that for linear elastic rods of length l providing the transversal connection (characterized by the product EI between the Young modulus and the moment of inertia of the cross section) the transversal stiffness is

$$s = 24\frac{EI}{l^3}, \tag{1}$$

where the columns have been assumed to be massless, so that their inertia is neglected.[1]

In the structural interface, all transversal links between masses are assumed to be faulted up to the position corresponding to the j^*th cell. In this configuration, the equations of motion for the structure can be written as

$$\begin{aligned} &-M_-\ddot{u}_-^{(j)} - sH(j-j^*)[\![u^{(j)}]\!] + c\left(u_-^{(j+1)} + u_-^{(j-1)} - 2u_-^{(j)}\right) = -\delta_{jn^*}Q, \\ &-M_+\ddot{u}_+^{(j)} + sH(j-j^*)[\![u^{(j)}]\!] + c\left(u_+^{(j+1)} + u_+^{(j-1)} - 2u_+^{(j)}\right) = \delta_{jn^*}Q, \end{aligned} \tag{2}$$

where j^* denotes the cell corresponding to the "tip of the fault" and

$$[\![u^{(j)}]\!] = u_-^{(j)} - u_+^{(j)} \tag{3}$$

is the jump in displacement across the structural interface, Q is a shear force applied to the n^* cell (at a distance D to j^*), and $H(j-j^*)$ and δ_{jn^*} are the step function and the Kronecker symbol, respectively.

Here the step function is defined such that $H(j-j^*) = 0$ for $j < j^*$, and $H(j-j^*) = 1$ for $j \geq j^*$. Note that both j^* and n^* are functions of time when the fault propagates with velocity V, so that

$$j^*(t) = Vt, \tag{4}$$

where V has the dimension of the inverse of a time and can be regarded as the speed of a fault in a dimensionless discrete structure.

Our aim in the present article is the dynamical analysis of the propagation of the faulted zone within the structural interface. However, it is an instrumental premise to develop and solve (i) a continuous model for the interface and analyze (ii) the statics of the faulted structural interface and (iii) the time-harmonic dynamics of the intact (i.e., without faulted links) structural interface via the Bloch–Floquet technique (which is deferred to Appendix A).

3. Structural interface: A continuous model. A "continuous version" of the discrete model of interface introduced so far can be easily developed. To this purpose, the two rows of masses separated by discrete springs of stiffness c and placed at a distance d become a continuous axially deformable rod (for which the product EA between the elastic modulus and the area of the cross section is taken to be equal to $c\,d$) with linearly distributed mass $m = M/d$, while the cross links between the masses become a continuous distribution of Winkler-like springs of constant $\kappa = s/d$. Therefore, we provide the following relations:

$$EA = cd, \quad M = md, \quad s = \kappa d, \quad v = Vd, \quad Q = qd. \tag{5}$$

Equations (2) can therefore be rewritten (in a "condensed form" using the symbol $\pm$) as

$$-m_\pm\ddot{u}_\pm^{(j)} \pm \kappa H(j-j^*)[\![u^{(j)}]\!] + EA\frac{u_\pm^{(j+1)} + u_\pm^{(j-1)} - 2u_\pm^{(j)}}{d^2} = \pm\frac{\delta_{jn^*}Q}{d}, \tag{6}$$

[1]Strictly speaking, in the following we will not need to assume expression (1) for s, so that more complicated stiffnesses can be introduced, for instance, depending on a transversal prestress.

so that we obtain in the limit $d \longrightarrow 0$ the differential equations governing the dynamics of the continuous model

$$-m_{\pm}\ddot{u}_{\pm} \pm \kappa H(x - x_j)[\![u]\!] + EA\, u''_{\pm} = \pm q\delta(x - x^*), \tag{7}$$

where $u''_{\pm}$ denotes the second derivative of $u_{\pm}$ taken with respect to x, x_j is the position of the fault tip, x^* is the (negative) coordinate in which the force q is applied, and $\delta(x - x^*)$ is the Dirac delta.

For steady propagation of the fault and of the forces q with constant velocity v, we introduce the change of variables

$$\zeta = x - vt, \quad \text{so that} \quad \ddot{u}_{\pm} = v^2 u''_{\pm},$$

and equations (7) become

$$\left(EA - m_{\pm}v^2\right) u''_{\pm} \pm \kappa H(\zeta)[\![u]\!] = \pm q\, \delta(\zeta - \zeta^*), \tag{8}$$

where ζ^* is the distance between the applied load q and the fault tip in a moving coordinate system, so that the quasi-static case is immediately recovered for vanishing speed of the fault, $v = 0$.

Note that we have assumed that the speed of propagation of the fault, v, is smaller than the smallest of the speeds of propagation of longitudinal waves in the two rods $+$ and $-$, namely

$$v < v_{min} = \min\{v_+, v_-\}, \quad v_{\pm} = \sqrt{EA/m_{\pm}}. \tag{9}$$

The solution to (8) is

$$u_+(\zeta) = -\frac{q}{EA - m_+v^2} \begin{cases} \theta e^{-\zeta/\theta} & \text{for } \zeta \geq 0, \\ \theta - \zeta & \text{for } \zeta_* \leq \zeta \leq 0, \\ \theta - \zeta^* & \text{for } \zeta \leq \zeta^* \end{cases} \tag{10}$$

and

$$u_-(\zeta) = -\rho\, u_+(\zeta), \tag{11}$$

where

$$\theta = \theta(v) = \sqrt{\frac{EA - m_+v^2}{\kappa\,(1 + \rho)}}, \quad \rho = \rho(v) = \frac{EA - m_+v^2}{EA - m_-v^2}. \tag{12}$$

For the static case, one has

$$[\![u]\!](\zeta) = \frac{2q}{\kappa\theta_0} \begin{cases} \theta_0 e^{-\zeta/\theta_0} & \text{for } \zeta \geq 0, \\ \theta_0 - \zeta & \text{for } \zeta_* \leq \zeta \leq 0, \\ \theta_0 - \zeta^* & \text{for } \zeta \leq \zeta^*, \end{cases} \tag{13}$$

where

$$\theta_0 = \theta(0) = \sqrt{\frac{EA}{2\kappa}}. \tag{14}$$

Let us rewrite solution (10) in terms of the displacement jump in the case in which the force is placed at infinity as

$$[\![u]\!](\zeta) = \frac{2q}{\kappa\theta} \begin{cases} \theta e^{-\zeta/\theta} & \text{for } \zeta \geq 0, \\ \theta - \zeta & \text{for } \zeta \leq 0. \end{cases} \tag{15}$$

Computing the integral of the displacement jump along the intact part of the chain, we have

$$\int_0^\infty [\![u]\!](\zeta) d\zeta = \frac{q}{\kappa}, \tag{16}$$

so that, as expected, the applied force in the continuous model is proportional, through the stiffness κ, to the accumulated displacement jump.

Now, the analysis of the fault propagation in the continuous model under examination depends on the failure criterion chosen for the spring bed, so that we assume the following simple failure condition, setting a limit to the maximum displacement jump:

$$[\![u]\!](0) = U_{cr}. \tag{17}$$

From this criterion we can conclude that the propagation cannot be stable for a *fixed* force q. Indeed, for every force amplitude q which is high enough to break, say, the "first spring," the fault will propagate accelerating from zero to its maximum speed $v_{cr} = \min\{v_+, v_-\}$. This is a direct consequence of the fact that function (15) is a monotonically increasing function of v, blowing up in the limit $v \longrightarrow v_{cr}$.

A stable, steady-state propagation of a fault can be obtained only when the force q is *guided*, i.e., when its amplitude is "properly adjusted" during the motion. If the load is guided by

$$q(v) = \kappa U_{cr} \theta(v), \tag{18}$$

the speed will be a constant "neutral" value, so that any deviation will bring the velocity to a new value. Therefore, it becomes more effective to impose a certain desired speed of propagation $v = v_\circ < v_{cr}$ and to apply the moving load in the following way:

$$q(v) = \kappa U_{cr} \theta(v) f\left(\frac{\theta(v)}{\theta(v_\circ)}\right), \tag{19}$$

where f is any monotonically increasing function, so that a substitution of (19) into (15) evaluated in $\zeta = 0$ yields the following formula:

$$[\![u]\!](0) = U_{cr} f\left(\frac{\theta(v)}{\theta(v_\circ)}\right),$$

showing that an increase (decrease) in the speed decreases (increases) the jump, so that the fault is moved back to the prescribed steady-state velocity.

3.1. Structural interface: The discrete model. We are now in a position to attack the problem of the discrete model of the interface (Figure 1). It is instrumental first to solve the statics and later to develop the dynamical analysis.

3.1.1. Statics of the faulted structural interface. Without loss of generality, we now assume that the failure of transversal bonds runs up to the link labeled $j^* = 0$ (Figure 1). The equilibrium equations of the chain can be immediately obtained from equations (2) by eliminating the inertial terms

$$\begin{aligned} sH(j)[\![u^{(j)}]\!] - c\left(u_-^{(j+1)} + u_-^{(j-1)} - 2u_-^{(j)}\right) &= \delta_{jn^*}Q, \\ sH(j)[\![u^{(j)}]\!] + c\left(u_+^{(j+1)} + u_+^{(j-1)} - 2u_+^{(j)}\right) &= \delta_{jn^*}Q. \end{aligned} \tag{20}$$

We assume $n^* \le 0$, and we note that the static solution has to be skew-symmetric with respect to the center line of the structural interface, so that

$$u_+^{(j)} = -u_-^{(j)} \equiv -u^{(j)}, \quad [\![u^{(j)}]\!] = 2u^{(j)}. \tag{21}$$

Therefore, the system (20) becomes equivalent to the following discrete problem:

$$\begin{aligned} u^{(j+1)} + u^{(j-1)} - 2u^{(j)} &= -\frac{Q}{c}\delta_{jn^*}, && j < 0, \\ u^{(j+1)} + u^{(j-1)} - 2\left(1 + \frac{s}{c}\right)u^{(j)} &= -\frac{Q}{c}\delta_{jn^*}, && j \ge 0, \end{aligned} \tag{22}$$

complemented with the conditions at infinity:

$$\begin{aligned} u^{(j)} &\to U_\infty, && j \to -\infty, \\ u^{(j)} &\to 0, && j \to \infty. \end{aligned} \tag{23}$$

It may be easily observed that all springs on the left of the applied forces Q are unloaded, so that the masses simply suffer the rigid body motion

$$u^{(j)} \equiv U_\infty, \quad j \le n^*. \tag{24}$$

Therefore, the solution to the problem (22) is

$$u^{(j)} = \frac{Q}{c}W_{n^*}(j), \quad W_{n^*}(\eta) = \begin{cases} u_0 e^{\eta \ln \lambda}, & \eta \ge 0, \\ u_0 - \eta, & n^* \le \eta \le 0, \\ u_0 - n^*, & \eta \le n^*, \end{cases} \tag{25}$$

where $W_{n^*} \in C(-\infty, \infty)$ is considered a function of the continuous variable η, $U_\infty = (u_0 - n_*)Q/c$, and parameters u_0 and $0 < \lambda < 1$ are given by

$$\begin{aligned} \lambda &= 1 + \frac{s}{c} - \sqrt{\left(1 + \frac{s}{c}\right)^2 - 1}, \\ u_0 &= -\frac{1}{1 + \lambda - 2\left(1 + \frac{s}{c}\right)} = \frac{\lambda}{1 - \lambda} > 0. \end{aligned} \tag{26}$$

Note that if the load is brought at infinity ($n^* \to -\infty$), U_∞ blows up to infinity, too, yielding a limit solution in the following form:

$$[\![u^{(j)}]\!] = W_\infty(j), \quad W_\infty(\eta) = \frac{2Q}{c}\begin{cases} u_0 e^{\eta \ln \lambda}, & \eta \ge 0, \\ u_0 - \eta, & \eta \le 0. \end{cases} \tag{27}$$

Finally, the total displacement of the structural interface from the fault tip to infinity can be calculated to be

$$\sum_{j=0}^{\infty} u_j = \frac{2Q}{c}\frac{u_0\lambda}{(1-\lambda)^2} = \frac{Q}{s}, \tag{28}$$

a result that can be checked from simple mechanical considerations.

A link to the continuous model. The relationship between the discrete and continuous formulations follows from definitions (5) and from a comparison between (13) and (25):

$$\zeta = \eta\, d, \tag{29}$$

so that the equations (13) for the continuous system become

$$[\![u]\!](\eta) = \frac{2Q}{c}\begin{cases} \sqrt{\dfrac{c}{2s}}e^{-\sqrt{\frac{2s}{c}}\eta} & \text{for } \eta \geq 0, \\ \sqrt{\dfrac{c}{2s}} - \eta & \text{for } \eta_* \leq \eta \leq 0, \\ \sqrt{\dfrac{c}{2s}} - \eta^* & \text{for } \eta \leq \eta^*. \end{cases} \tag{30}$$

For small s/c the relationships

$$\ln\lambda = -\sqrt{\frac{2s}{c}} + O\left(\frac{s}{c}\right), \quad u_0 = \sqrt{\frac{c}{2s}} + O(1) \tag{31}$$

show that (30) coincides with (25) in the limit of vanishing transversal stiffness.

We note that, with the parameter identification (5) and (29), if the load is brought to (minus) infinity, the main asymptotic terms determining the load intensity are the same for both the discrete and continuous models. We will exploit this property to normalize the solution for the dynamic propagation in the discrete structure when the load is prescribed at infinity. In this case, (15) becomes

$$[\![u]\!](\eta) = \frac{2Q}{c}\mathcal{S}\begin{cases} \theta_c e^{-\eta/\theta_c} & \text{for } \eta \geq 0, \\ \theta_c - \eta & \text{for } \eta \leq 0, \end{cases} \tag{32}$$

where, since $\theta(v) = \theta_c(V)d$, we define

$$\mathcal{S} = \mathcal{S}(V) = \frac{1}{2}\left(\frac{V_+^2}{V_+^2 - V^2} + \frac{V_-^2}{V_-^2 - V^2}\right), \quad \theta_c = \theta_c(V) = \sqrt{\frac{c}{2s}}\frac{1}{\sqrt{\mathcal{S}(V)}}. \tag{33}$$

3.1.2. Dynamics of the faulted structural interface. Let us now assume that a failure of transversal bonds is traveling in the structural interface at a constant speed V as a result of a faraway applied loading (as $n^* \to -\infty$); see Figure 1. The equations of motion in the discrete system defining the interface become

$$\begin{aligned} -M_-\ddot{u}_-^{(j)} - sH(j-j^*)[\![u^{(j)}]\!] + c\left(u_-^{(j+1)} + u_-^{(j-1)} - 2u_-^{(j)}\right) = 0, \\ -M_+\ddot{u}_+^{(j)} + sH(j-j^*)[\![u^{(j)}]\!] + c\left(u_+^{(j+1)} + u_+^{(j-1)} - 2u_+^{(j)}\right) = 0. \end{aligned} \tag{34}$$

It is also assumed that the velocity of the fault propagation V is smaller than the minimum of the two velocities (see (A.6)) of propagation in the two upper and lower discrete structures forming the interface, taken to be transversally disconnected, namely,

$$V < V_{cr} = \min\{V_-, \quad V_+\}. \tag{35}$$

Now, following Slepyan (2002), the discrete problem equations (2) are transformed into a problem depending with continuity on the variable

$$\eta = j - Vt, \tag{36}$$

denoting a dimensionless coordinate taken from cell j^*. It is assumed therefore that

$$u_\pm^{(j)} = u_\pm^{(j)}(\eta) \quad \text{and} \quad u_\pm^{(j\pm1)} = u_\pm^{(j)}(\eta \pm 1), \tag{37}$$

so that

$$\ddot{u}^{(j)} = \frac{\partial^2 u(\eta)}{\partial t^2} = V^2 u''(\eta), \tag{38}$$

and, finally, we obtain a "continuous version" of the equations of motion (2):

$$\begin{aligned} &-V^2 M_- u_-''(\eta) - sH(\eta)[\![u(\eta)]\!] + c\,[u_-(\eta+1) + u_-(\eta-1) - 2u_-(\eta)] = 0,\\ &-V^2 M_+ u_+''(\eta) + sH(\eta)[\![u(\eta)]\!] + c\,[u_+(\eta+1) + u_+(\eta-1) - 2u_+(\eta)] = 0. \end{aligned} \tag{39}$$

It may be worth noting that the solution of problem (39) must satisfy specific conditions at infinity. Namely, since a steady-state regime is analyzed, waves may propagate to plus and minus infinity, so that the solution at infinity does not decay in both directions.

Now introducing the Fourier transform in a distributional sense,

$$\bar{u}(k) = \int_{-\infty}^{+\infty} u(\eta) e^{ik\eta}\, d\eta, \tag{40}$$

so that the properties

$$\bar{u}''(k) = (0+ik)^2 \bar{u}(k), \qquad e^{\pm ik}\,\bar{u}(k) = \int_{-\infty}^{+\infty} u(\eta \pm 1) e^{ik\eta}\, d\eta \tag{41}$$

hold, where

$$(0+ik) = \lim_{\epsilon \to +0} (\epsilon + ik)$$

(details on the causality principle are given by Slepyan (2002)), we obtain for equations (39) the following expressions in the transformed domain:

$$\begin{aligned} &-(0+ik)^2 V^2 M_- \bar{u}_-(k) - s\Psi^+(k) + 2c(\cos k - 1)\bar{u}_-(k) = 0,\\ &-(0+ik)^2 V^2 M_+ \bar{u}_+(k) + s\Psi^+(k) + 2c(\cos k - 1)\bar{u}_+(k) = 0, \end{aligned} \tag{42}$$

where we have introduced the notation

$$\Psi^+(k) = \int_0^{+\infty} [\![u(\eta)]\!] e^{ik\eta}\, d\eta, \quad \Psi^-(k) = \int_{-\infty}^{0} [\![u(\eta)]\!] e^{ik\eta}\, d\eta, \tag{43}$$

so that the decomposition of the full Fourier transform takes place:

$$[\![\bar{u}(k)]\!] = \Psi^+(k) + \Psi^-(k). \tag{44}$$

The displacement jump $[\![u(\eta)]\!]$ behaves at infinity as the original functions $u_-(\eta)$ and $u_+(\eta)$; therefore, $\Psi^+(k)$ is analytical in the upper half plane $\operatorname{Im} k > 0$. In the limit case $\epsilon \to 0$, function $\Psi^+(k)$ can have poles on the real axis corresponding to waves traveling from the fault tip to plus infinity along the part of the interface where links are still active. In turn, the function $\Psi^-(k)$ is analytical in the lower half plane $\operatorname{Im} k < 0$ and can have poles along the real axis corresponding to possible waves traveling along both parts of the discrete structure where links have been broken. Finally, the function $\Psi^-(k)$ can have a pole at the point $k = 0$ induced by remotely applied forces.

The jump function $[\![u(\eta)]\!]$ is a continuous function of η, smooth in both regions $(-\infty, 0)$ and $(0, \infty)$. If we define its value at zero point as

$$[\![u(0)]\!] = U_0, \tag{45}$$

then the standard stationary phase approximation leads to the following asymptotic estimate for the one-sided Fourier transforms:

$$\Psi^{\pm}(k) = \pm i\frac{U_0}{k} + O\left(\frac{1}{k^2}\right), \quad \operatorname{Im} k \to \pm\infty. \tag{46}$$

Now summing and subtracting equations (42) and taking into account (44), we obtain

$$\langle \bar{u}(k) \rangle = \frac{m_*}{\Phi(k)} [\![\bar{u}(k)]\!] \tag{47}$$

and the Wiener–Hopf problem

$$\mathcal{Q}_+(k)\,\Psi^+(k) + \mathcal{Q}_-(k)\,\Psi^-(k) = 0, \tag{48}$$

where the jump operator has been defined by (3) and the average operator $\langle\rangle$ is used here in the usual manner, $\langle f \rangle = (f_+ + f_-)/2$, while functions Φ, $\mathcal{Q}_+$, and $\mathcal{Q}_-$ are defined as

$$\Phi(k) = -\frac{(0+ik)^2 + 4c_*\,(1-\cos k)}{(0+ik)^2} \tag{49}$$

and

$$\mathcal{Q}_-(k) = \Phi^2(k) - m_*^2, \quad \mathcal{Q}_+(k) = \Phi^2(k) - m_*^2 - \frac{4s_*}{(0+ik)^2}\Phi(k). \tag{50}$$

In (47)–(50) we have introduced the following dimensionless parameters:

$$s_* = \frac{s}{V^2\,\langle M \rangle}, \quad c_* = \frac{c}{V^2\,\langle M \rangle}, \quad m_* = \frac{[\![M]\!]}{\langle M \rangle}, \tag{51}$$

where we note that for every $V < V_{cr}$ the following inequalities hold true:

$$m_* \in (-1, 1), \quad 2c_* - 1 > |m_*|. \tag{52}$$

The formulated Wiener–Hopf problem is homogeneous and therefore admits an infinite number of solutions, so that we assume the same loading condition at infinity as determined for quasi-static loading of the continuous system (see (32)), which yields

$$\Psi^-(k) = -\frac{2Q}{ck^2}\mathcal{S}(V), \quad k \to 0, \tag{53}$$

a condition enforcing uniqueness.

The function $\Phi(k)$ is bounded along the entire real axis R and in the limit case $\epsilon = 0$ displays the following asymptotic properties:

$$\Phi(k) = -1 + O\left(\frac{1}{k^2}\right), \quad k \to \infty, \tag{54}$$

and

$$\Phi(k) = 2c_* - 1 + O\left(k^2\right), \quad k \to 0. \tag{55}$$

Moreover, function $\Phi(k)$ has a finite number of zeroes (at least one) on the positive part of the real axis, $k = \alpha_1, \alpha_2, \ldots, \alpha_n$, $\alpha_i > 0$.

The even functions $\mathcal{Q}_+(k)$ and $\mathcal{Q}_-(k)$ behave at infinity as

$$\mathcal{Q}_\pm(k) = 1 - m_*^2 + O\left(\frac{1}{k^2}\right), \quad k \to \infty, \tag{56}$$

and near the origin as

$$\mathcal{Q}_-(k) = (2c_* - 1)^2 - m_*^2 + O(k^2), \quad \mathcal{Q}_+(k) = (2c_* - 1)\frac{4s_*}{k^2} + O(1), \quad k \to 0. \tag{57}$$

Zeroes of the functions $\mathcal{Q}_\pm(k)$ and the solution of the Wiener–Hopf problem. The solution of the Wiener–Hopf problem requires a detailed analysis of the zeroes of the functions $\mathcal{Q}_\pm(k)$. These can be computed in the following implicit way. First, the equation $\mathcal{Q}_-(k) = 0$ can be directly checked to be equivalent to the following two equations:

$$kV = 2V\sqrt{\frac{2c_*}{1 \pm m_*}}\left|\sin\frac{k}{2}\right|, \tag{58}$$

which can be simplified to

$$kV = 2V_\pm\left|\sin\frac{k}{2}\right|. \tag{59}$$

Second, the equation $\mathcal{Q}_+(k) = 0$ is equivalent to the following (two, corresponding to the $\pm$) equations:

$$k = \sqrt{\frac{a(k) \pm \sqrt{a^2(k) - b(k)}}{1 - m_*^2}}, \tag{60}$$

where

$$a(k) = 2\left(s_* + 2c_*\sin^2\frac{k}{2}\right), \quad b(k) = 8c_*(1 - m_*^2)\sin^2\frac{k}{2}\left(s_* + 2c_*\sin^2\frac{k}{2}\right), \tag{61}$$

a condition which, employing functions $\beta(k)$ and $\gamma(k)$ defined by equations (A.5), can be rewritten in the form

$$kV = \sqrt{V_+V_-}\sqrt{\beta(k) \pm \sqrt{\beta^2(k) - \gamma(k)}} \tag{62}$$

when the definitions (51) and the identities

$$\frac{2c_*}{\sqrt{1-m_*^2}} = \frac{V_+V_-}{V^2}, \quad \frac{1}{\sqrt{1-m_*^2}} = \frac{1}{2}\left(\sqrt{\frac{M_+}{M_-}} + \sqrt{\frac{M_-}{M_+}}\right)$$

are taken into account.

Taking $\omega_\pm = kV$ and $hd = k$, (59) and (62) coincide, respectively, with (A.7) and (A.4), the latter two equations providing the frequencies for which the structural interface vibrates in the two limit cases of fully broken and completely intact links (two equations obtained through a Bloch–Floquet analysis in Appendix A). This observation suggests a methodology for determining the zeroes of the functions $\mathcal{Q}_\pm(k)$ from the dispersion diagram of the Bloch–Floquet analysis. Namely, the zeroes can be located through the intersection between the dispersion curves and the straight line $\omega = Vk$. Obviously, this methodology works if an intersection exists between the Bloch–Floquet branches and the line, which can be proved for every velocity V smaller than V_{cr}.

The Wiener–Hopf problem (48) can be rewritten as

$$\Psi^+(k)L(k) + \Psi^-(k) = 0, \tag{63}$$

where the even function of the real argument k,

$$L(k) = \frac{\mathcal{Q}_+(k)}{\mathcal{Q}_-(k)} = 1 - \frac{4s_*\Phi(k)}{(0+ik)^2\big(\Phi^2(k) - m_*^2\big)}, \tag{64}$$

exhibits the asymptotics

$$L(k) = 1 + O\left(\frac{1}{k^2}\right), \quad k \to \infty,$$

and has a double pole at the point $k = 0$:

$$L(k) = \frac{l_0^2}{k^2} + O(1), \quad k \to 0, \quad l_0 = 2\sqrt{\frac{s_*(2c_*-1)}{(2c_*-1)^2 - m_*^2}}.$$

The factorization of the function $L(k)$ becomes easier by employing the following form:

$$L(k) = \frac{k^2 + l_0^2}{k^2} L_0(k), \tag{65}$$

where

$$L_0(k) = 1 + O(k^2), \quad k \to 0, \quad L_0(k) = 1 + O\big(k^{-2}\big), \quad k \to \pm\infty, \tag{66}$$

so that we introduce the factorization of the function $L_0(k)$ as

$$L_0(k) = \frac{L_0^+(k)}{L_0^-(k)}, \quad L_0^\pm(k) = \exp\left[\frac{1}{2\pi i}\int_{-\infty}^{\infty} \frac{\log L_0(t)}{t-k}\,dt\right], \quad \pm \operatorname{Im} k > 0. \tag{67}$$

Moreover,

$$\lim_{k\to\infty} L_0^{\pm}(k) = 1, \quad L_0^{\pm}(k) = \mathcal{R}(1 - ipk) + O(k^2), \quad k \to 0, \tag{68}$$

where

$$\mathcal{R} = \exp\left\{\frac{1}{\pi}\int_0^{\infty} \frac{\mathrm{Arg}L_0(k)}{k}dk\right\}, \quad p = \frac{1}{\pi}\int_0^{\infty} \frac{\log|L_0(k)|}{k^2}dk, \tag{69}$$

and the integral defining p exists in view of (66). Let us note that according to (49)–(51) and (64) these parameters depend on the fault velocity: $\mathcal{R} = \mathcal{R}(V)$, $p = p(V)$.

Following Slepyan (2002), the Wiener–Hopf problem (48) can now be rewritten as

$$L^+\Psi^+ + L^-\Psi^- = C\left(\frac{1}{0 + ik} + \frac{1}{0 - ik}\right), \tag{70}$$

where the constant C defines the level of the load applied at infinity.

Using the factorization of the kernel function

$$L^+(k) = \frac{k + il_0}{k}L_0^+(k), \quad L^-(k) = \frac{k}{k - il_0}L_0^-(k),$$

we can find *the solution of the Wiener–Hopf problem* in the form

$$\Psi^{\pm}(k) = \frac{C}{L^{\pm}(k)}\frac{1}{0 \pm ik}. \tag{71}$$

3.2. A comparison between the continuous and discrete models of the interface. The asymptotics of the solution to the Wiener–Hopf problem (71) allows us to determine (i) the unknown constant C and to draw conclusions about (ii) the jump in displacement at the tip of the fault, (iii) the accumulated jump in displacement in the intact zone of the interface, and (iv) the leading term of asymptotics of the displacement jump at $-\infty$. These conclusions are listed below:

- Comparing the asymptotic behavior of the solution (71)

$$\Psi^-(k) = \frac{Cl_0}{\mathcal{R}k^2} + i\frac{C(1 + pl_0)}{\mathcal{R}k} + O(1), \quad k \to 0, \tag{72}$$

with (53) allows us to compute the unknown constant C as

$$C = -\frac{2Q\mathcal{R}}{l_0 c}\mathcal{S}(V). \tag{73}$$

- Comparing the asymptotic behavior of the solution (71)

$$\Psi^{\pm}(k) = \frac{C}{0 \pm ik}, \quad k \to \infty, \tag{74}$$

with (46) allows us to determine the displacement jump at the fault tip $U_0 = -C$ as

$$U_0 = [\![u]\!](0) = \frac{2Q}{c}\mathcal{S}\theta_d, \quad \theta_d = \mathcal{R}\theta_c, \tag{75}$$

where we have taken into account that $l_0 = \theta_c^{-1}$.

- Comparing the asymptotic behavior of the solution (71)

$$\Psi^+(k) = -\frac{C}{l_0\mathcal{R}} + O(k), \quad k \to 0, \tag{76}$$

with (43) allows us to evaluate the accumulated displacement jump in the intact part of the structural interface as

$$\int_0^\infty [\![u]\!](\eta)d\eta = \Psi^+(0) = \frac{Q}{s}, \tag{77}$$

showing that the total force is equal to the accumulated displacement jump multiplied by the transversal stiffness, as in the cases represented by (16) and (28).

- Finally, the behavior of the jump in displacements across the interface at $-\infty$ can be evaluated using once again (72):

$$[\![u]\!](\eta) = \frac{2Q}{c}\big(\theta_c + p - \eta\big)\mathcal{S} + \mathcal{U} \quad \text{as} \quad \eta \to -\infty, \tag{78}$$

where $\mathcal{U}$ is a bounded function of η, corresponding to oscillatory terms related to the zeroes of the function $\mathcal{Q}_-$ along the real axis.

Now we are in a position to compare the results of the dynamic analysis of the discrete model with those relative to the continuous model of the structural interface. This comparison is performed asymptotically when the transversal stiffness becomes small, so that, for every fixed value of $V < V_{cr}$, the relations

$$\mathcal{R} \to 1, \quad p \to 0, \quad \mathcal{U} \to 0, \quad \text{as} \quad s/c \to 0,$$

show that (75) and (78) coincide with (32), respectively, in the limits $\eta \longrightarrow 0$ and $\eta \longrightarrow -\infty$. Therefore the discrete model converges to the continuous one.

4. Numerical results and discussion. The numerical solution of $(69)_1$ allows an evaluation of the discontinuity of displacement at the fault tip as a function of the fault tip velocity. This is linked to an estimate of the energy release rate and related to the stability of the fault propagation. We begin with a discussion on the Bloch–Floquet structure of the problem (Appendix A), together with the numerical evaluation of $L_0(k)$ from (65), providing an important preliminary qualitative interpretation of results.

Waves generated by the fault. By evaluating zeroes of the functions $\mathcal{Q}_\pm(k)$ from (48) we obtain the dispersion equations for waves, which are supported by the discrete structure without the fault.

Equations (58) and (62) lead to the dispersion relations

$$\omega_1^\pm = 2V_\pm \left|\sin\frac{k}{2}\right|, \quad \omega_2^\pm = \sqrt{V_+V_-}\sqrt{\beta^2(k) - \gamma(k)}. \tag{79}$$

The graphs of ω versus k are shown in Figure 3(a)–(b) as dispersion curves for Bloch–Floquet waves, which would correspond to propagation behind ($\omega_1^\pm(k)$) or ahead ($\omega_2^\pm(k)$) of the fault tip. The computations are relative to the contrast $M_+/M_- = 4$ and the stiffness ratios $s/c = 4$ and $s/c = 0.2$ employed for Figure 3(a)–(b), respectively.

For waves ahead of the fault tip the dashed dispersion curves in Figure 3(a) are separated by a finite width stop band. The width of this stop band decreases with

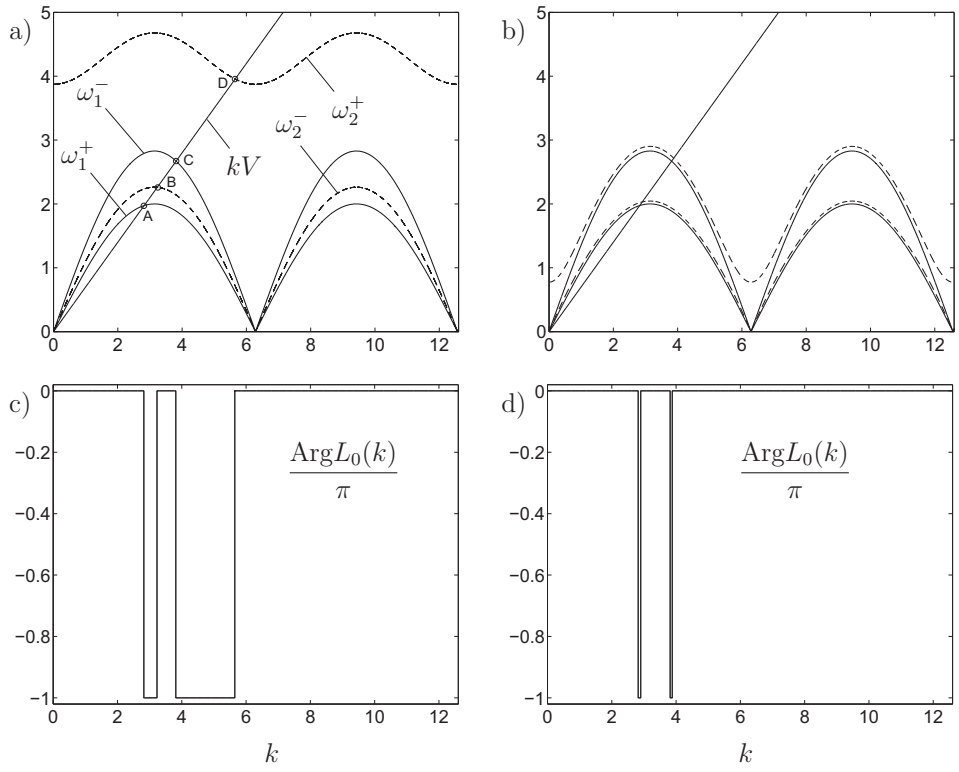

FIG. 3. *Dispersion diagrams, determination of the zeroes of the functions* $\mathcal{Q}_\pm(k)$. *Computations are reported for* $M_+/M_- = 4$, $s/c = 4$, *and* $s/c = 0.2$ *in* (a) *and* (b), *respectively. Evaluations of the functions* $\mathrm{Arg}L_0(k)$ *are reported in* (c) *and* (d), *corresponding to the two cases* (a) *and* (b).

the decrease of the stiffness ratio s/c, so that no stop bands are visible in Figure 3(b), relative to $s/c = 0.2$.

The straight line $\omega = Vk$ is shown in Figure 3(a)–(b), where V is the speed of the propagating fault. The points of intersection of this straight line with the dispersion curves characterize the waves generated by the propagating fault as it breaks the link between the upper and lower discrete structures. Each point of intersection corresponds to a jump in $\mathrm{Arg}\, L_0(k)$, as shown in Figure 3(c)–(d). Points labeled as A, B, C, and D in Figure 3(a) can be described as follows. Points A and C represent two waves behind the tip of the fault, and their group velocities are positive and negative, respectively. Namely, the wave corresponding to A propagates behind the fault tip with a low positive group velocity, whereas the wave corresponding to C has a negative group velocity, and hence it carries the energy away from the tip of the fault. Points B and D show the intersection of the line $\omega = kV$ with the dashed dispersion curves. They do not represent any wave emanating ahead of the fault, since the group velocity at D is negative, which would correspond to a wave carrying the energy back to the fault tip, and the group velocity at B is null, which corresponds to a standing wave.

Figure 4 is identical to Figure 3, except that we have reported two additional straight lines, namely, $\omega = kV_1$ and $\omega = kV_2$ for $V > V_1 > V_2$. The tangent lines to the dispersion curves at E and F have the same slope as V_1 and V_2, respectively;

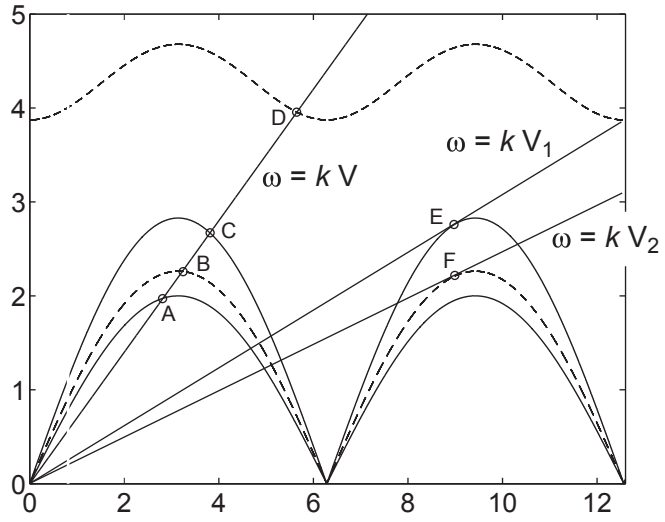

FIG. 4. *Dispersion diagrams for $s/c = 4$ as in Figure* 3(a). *Points* E *and* F *represent the resonant modes where the group velocity of the wave generated by the fault coincide with the speed V of the fault.*

i.e., the group velocities of the waves corresponding to E and F coincide with the propagation speed of the fault. These modes can be characterized as resonant modes. Furthermore, it is noted that for $V > V_1$ the propagating fault does not generate any wave ahead of the its tip, with the group velocity exceeding V. It will be apparent that this regime corresponds to possible stable propagation.

Stability of the propagating fault. The normalized displacement jump in the lattice fault versus the fault speed is shown in Figure 5 for different values of the speed ratios s/c. The response of the continuous model is also reported (dashed). The oscillatory behavior of θ_d for small values of V is linked to the oscillations of Arg L_0, as illustrated in Figure 3(c)–(d). In the physical configuration, it corresponds to the instability of the fault. Note that all the graphs initiate at the values (indicated by small circles on the vertical axis) obtained from the quasi-static solution of the discrete model (27). For larger values of the fault speed, the quantity θ_d becomes a monotonically decreasing function of the fault speed V, and hence in this case the fault propagation is stable at constant speed, provided the external load can be controlled according to (19). The numerical computations in Figure 5 suggest that small values of s/c correspond to a wider interval of the values of V describing a stable propagation of the fault. Finally, following a complex motivation provided by Slepyan (2002), we note that the quantity shown in Figure 5 can also have a link to the dissipation energy carried by the waves initiated by the propagating fault.

Figure 5 emphasizes the differences between the continuous and discrete models of fault propagation. The ratio between the displacement jumps at the fault tip in the discrete and continuous models of the fault is equal to $\mathcal{R} = \theta_d/\theta_c$, where $\mathcal{R}$ is determined by $(69)_1$. The discrete model is characterized in Figure 5 by intrinsic instability for small values of V, corresponding to the highly oscillatory part of the graphs. This feature does not appear in the continuous model and is directly related to the discrete nature of the structural interface, a feature that represents the dispersion inherent to a discrete system.

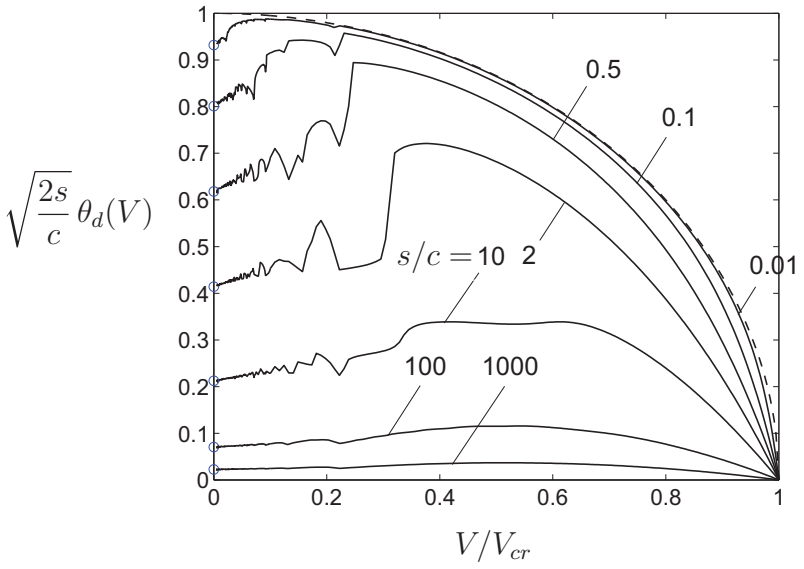

FIG. 5. *Normalized displacement jump at the fault tip,* $\sqrt{s/(2c)}U_0/(Q\mathcal{S}(V))$ *(compare with* (75)*), computed for equal masses* $M_+ = M_-$*. The quasi-static solutions of the discrete interface model are reported on the vertical axis and denoted by small circles. The dashed line is the solution of the continuous model of the interface and corresponds to* $\theta_c(V)\sqrt{2s/c}$*. The solid lines represent dynamical solutions of the discrete model of the interface for different values of the dimensionless parameter* s/c*.*

Appendix A. Bloch–Floquet analysis of the intact chain. In the absence of any failure of the transversal connections, the equations of motion of the structural interface shown in Figure 1 (nodes $j-1$, j, and $j+1$) are

$$\begin{aligned} &M_-\ddot{u}_-^{(j)} + s[\![u^{(j)}]\!] - c\left(u_-^{(j+1)} + u_-^{(j-1)} - 2u_-^{(j)}\right) = 0,\\ &M_+\ddot{u}_+^{(j)} - s[\![u^{(j)}]\!] - c\left(u_+^{(j+1)} + u_+^{(j-1)} - 2u_+^{(j)}\right) = 0. \end{aligned} \tag{A.1}$$

We assume the Bloch–Floquet form of solution

$$u_\pm^{(j+1)} = u_\pm^{(j)} e^{ihd}, \quad u_\pm^{(j)} = U_\pm e^{-i\omega t}, \tag{A.2}$$

where ω is the circular frequency and h the Bloch parameter, so that, through substitution in equations (A.1), we arrive at the algebraic problem

$$\begin{pmatrix} \omega^2 M_- - s + 2c(\cos hd - 1) & s \\ s & \omega^2 M_+ - s + 2c(\cos hd - 1) \end{pmatrix} \begin{pmatrix} U_- \\ U_+ \end{pmatrix} = \boldsymbol{0}, \tag{A.3}$$

which admits the following nontrivial solutions (expressed in nondimensional form):

$$\omega = \omega_2^{\pm}(hd) = \sqrt{V_+V_-}\sqrt{\beta(hd) \pm \sqrt{\beta^2(hd) - \gamma(hd)}}, \tag{A.4}$$

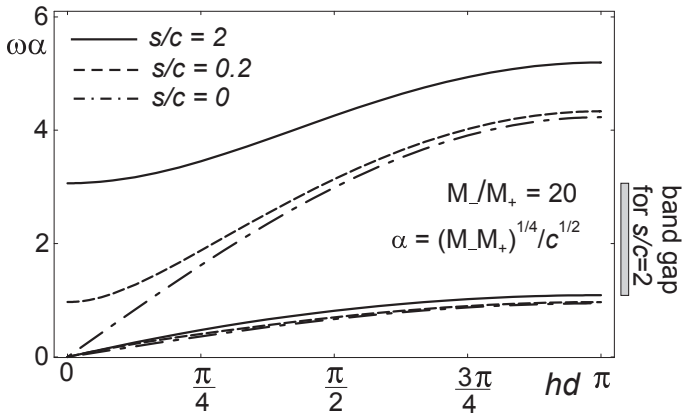

FIG. 6. *Dispersion diagram for the intact structural interface shown in Figure* 1.

where

(A.5)
$$\beta(\xi) = \frac{1}{2}\left(\sqrt{\frac{M_-}{M_+}} + \sqrt{\frac{M_+}{M_-}}\right)\left(\frac{s}{c} + 4\sin^2\frac{\xi}{2}\right), \quad \gamma(\xi) = 8\left(\frac{s}{c} + 2\sin^2\frac{\xi}{2}\right)\sin^2\frac{\xi}{2}$$

and

(A.6)
$$V_- = \sqrt{\frac{c}{M_-}}, \quad V_+ = \sqrt{\frac{c}{M_+}}.$$

Dispersion curves ω, made dimensionless through multiplication by

$$\alpha = \frac{(M_- M_+)^{1/4}}{c^{1/2}}$$

as functions of hd, can be plotted from (A.4) for each value of parameters s/c and M_-/M_+. Results relative to high contrast $M_-/M_+ = 20$ are reported in Figure 6 for s/c equal to 0, 0.2, and 2. It can be noted from Figure 6 that there is no transversal connection between masses when $s/c = 0$, so that in this case the dispersion curves for two separate arrays of masses are retrieved, in which waves propagate horizontally with the speeds (A.6). Obviously, there is no band gap in this case (when masses are disconnected), and the band gap is also absent for $s/c = 0.2$. However, there is a wide band gap in the case $s/c = 2$ at high mass contrast. We finally note that, differently from the diatomic crystal structure (see, for instance, Kittel (1971)), the optical phonon branches for $s/c = 0.2$ and 2 are increasing functions of the Bloch–Floquet parameter hd.

In the case when there are no transversal links between masses, $s/c = 0$, the frequencies at which waves propagate are

(A.7)
$$\omega = \omega_1^{\pm} = 2\sqrt{\frac{c}{M_\pm}}\left|\sin\frac{hd}{2}\right| = 2V_\pm\left|\sin\frac{hd}{2}\right|,$$

so that, assuming $M_- < M_+$ ($V_+ < V_-$), the following separation property holds:

(A.8)
$$\omega_1^+ < \omega_2^- < \omega_1^- < \omega_2^+.$$

In case $M_+ = M_-$, the first three branches of the dispersion diagram coincide.

Finally, we note that, as $s/c \to 0$, the distance between the dispersion curves vanishes, namely,

$$\text{dist}\{\omega_2^{\pm}(s/c) - \omega_1^{\pm}(s/c)\} \to 0, \quad s/c \to 0. \tag{A.9}$$

Acknowledgment. This work was initiated during the authors' stay in Edinburgh with the ICMS "research-in-group" grant.

REFERENCES

K. Bertoldi, D. Bigoni, and W. J. Drugan (2007a), *Structural interfaces in linear elasticity. Part I: Nonlocality and gradient approximations*, J. Mech. Phys. Solids, 55, pp. 1–34.

K. Bertoldi, D. Bigoni, and W. J. Drugan (2007b), *Structural interfaces in linear elasticity. Part II: Effective properties and neutrality*, J. Mech. Phys. Solids, 55, pp. 35–63.

K. Bertoldi, D. Bigoni, and W. J. Drugan (2007c), *A discrete-fibers model for bridged cracks and reinforced elliptical voids*, J. Mech. Phys. Solids, 55, pp. 1016–1035.

D. Bigoni and A. B. Movchan (2002), *Statics and dynamics of structural interfaces in elasticity*, Int. J. Solids Structures, 39, pp. 4843–4865.

M. Brun, A. B. Movchan, and N. V. Movchan (2010), *Shear polarisation of elastic waves by a structured interface*, Contin. Mech. Thermodyn., 22, pp. 663–677.

M. Gei (2008), *Elastic waves guided by a material interface*, Eur. J. Mech. A Solids, 27, pp. 328–345.

C. Kittel (1971), *Introduction to Solid State Physics*, 4th ed., John Wiley & Sons, New York.

P. A. Martin (2006), *Discrete scattering theory: Green's function for a square lattice*, Wave Motion, 43, pp. 619–629.

P. G. Martinsson and G. J. Rodin (2002), *Asymptotic expansions of lattice Green's functions*, R. Soc. Lond. Proc. Ser. A Math. Phys. Eng. Sci., 458, pp. 2609–2622.

G. S. Mishuris, A. B. Movchan, and L. I. Slepyan (2008), *Dynamical extraction of a single chain from a discrete lattice*, J. Mech. Phys. Solids, 56, pp. 487–495.

G. S. Mishuris, A. B. Movchan, and L. I. Slepyan (2009), *Localised knife waves in a structured interface*, J. Mech. Phys. Solids, 57, pp. 1958–1979.

A. B. Movchan, R. Bullough, and J. R. Willis (2003), *Two-dimensional lattice models of the Peierls type*, Phil. Mag., 83, pp. 569–587.

A. B. Movchan and L. I. Slepyan (2007), *Band gap Green's functions and localized oscillations*, R. Soc. Lond. Proc. Ser. A Math. Phys. Eng. Sci., 463, pp. 2709–2727.

L. I. Slepyan (2002), *Models and Phenomena in Fracture Mechanics*, Springer-Verlag, Berlin.

L. I. Slepyan (2005), *Crack in a material-bond lattice*, J. Mech. Phys. Solids, 53, pp. 1295–1313.

H. F. Zhao, D. E. Makarov, and G. J. Rodin (2011), *The resistance curve for subcritical cracks near the threshold*, Int. J. Fracture, 167, pp. 147–155.